Wideband Optical Vector Analysis Based on Microwave Photonic Frequency Downconversion

Meihui Cao, Ting Qing, Lihan Wang, Shupeng Li, Yijie Fang, Xiaohu Tang, Xufeng Chen, Ping Li, and Shilong Pan, *Senior Member, IEEE*

***Abstract*— A high-resolution optical vector analyzer (OVA) with wide measurement bandwidth based on microwave photonic frequency downconversion is proposed and experimentally demonstrated. In the proposed OVA, two pairs of frequency-swept dual-tone signals with different frequency intervals are used as the probe light. After passing through a device under test (DUT), the probe light is transmitted into a low-speed photodetector to perform frequency downconversion. Then, an intermediate frequency (IF) photocurrent with a fixed frequency is generated, which carries the DUT response. Hence, a low-speed electrical phase-magnitude detector (EPMD) can be employed to extract the magnitude and group delay responses of the DUT. Compared with the OVAs using the high-speed PD and ultrawide EPMD, the proposed approach is low-cost and has a high signal-to-noise ratio. In an experiment, the probe light is generated by the 2nd-order nonlinearity of the electro-optic modulator. Therefore, compared with conventional OVAs based on optical single-sideband (OSSB) or optical double-sideband (ODSB) modulation, the proposed OVA can achieve wide measurement bandwidth, which is four times (or two times) of that of the OSSB-based OVA (or the ODSB-based OVA). A frequency resolution of 6 MHz and a measurement bandwidth of 120 GHz are achieved.**

***Index Terms*— Optical vector analyzer, high-resolution, optical response, frequency downconversion, group delay.**

I. Introduction

OPTICAL vector analysis is a technique to obtain the optical spectral response of optical devices with unknown parameters, such as microdisk resonators, on-chip optical signal processing, and fiber Bragg gratings. In the past few decades, optical vector analyzers (OVAs) based on swept-wavelength interferometry (SWI), phase-shift method, and microwave photonics (MWP) have been proposed and demonstrated to acquire the magnitude and phase responses of the optical devices.

The SWI method [1], [2] employs swept-wavelength interferometry to measure the magnitude and phase responses of an optical device under test (DUT). The advantage of this method is that it can measure the DUT with wide bandwidth and large dynamic range. However, due to the low frequency accuracy and repeatability of the tunable laser source (TLS), this method has a poor frequency resolution (typically several hundreds of MHz [1]). The phase-shift method [3]–[5] is achieved by a TLS and a Mach-Zehnder modulator (MZM). This method inherently has a simple structure, high stability, and wide measurement bandwidth, but the nonlinearity of the electro-optic modulation would introduce measurement errors. Restricted by the low frequency accuracy and stability of the TLS, this method also has a poor frequency resolution.

To improve the frequency resolution, a large number of OVAs based on MWP were proposed and implemented via electrical frequency sweeping and phase-magnitude detection. Optical single-sideband (OSSB) modulation [6]–[10] or optical double-sideband (ODSB) modulation [11]–[13] is usually used to convert the frequency scanning in the electrical domain to the optical domain. The OSSB-based OVA can realize a sub-Hz frequency resolution theoretically, and a 23.4-kHz resolution has been reported [8]. However, since only one sideband is used to scan the spectrum, the measurement bandwidth is usually less than 40 GHz, limited by the bandwidth of the used components. The residual 1st-order and high-order sidebands would introduce measurement errors, which reduces the accuracy of the measurement results. Compared with the OSSB-based OVA, the ODSB-based OVA has a doubled measurement bandwidth and higher accuracy. However, the measurement range cannot meet the measurement requirements of optical DUTs with large bandwidth, either. Therefore, OVAs using an optical frequency comb as the probe light [14] were proposed to improve the measurement range. However, all the approaches need high-speed photodetector and electrical phase-magnitude detector with wide frequency sweeping range, which makes the OVA complex, expensive, and difficult to establish.

In this Letter, we propose and demonstrate a novel MWP-based OVA based on microwave photonic frequency downconversion, featuring wide measurement bandwidth, high resolution, and low cost simultaneously. In the proposed OVA, two pairs of frequency-swept dual-tone signals with different frequency intervals are used as the probe light, which is generated by the 2nd-order nonlinearity of the electro-optic modulator. After passing through a DUT, a low-speed photodetector (PD) receives the probe light and converts it into an intermediate frequency (IF) photocurrent. Then, a low-speed electrical phase-magnitude detector (EPMD) is employed to extract the DUT's magnitude and phase information from the IF photocurrent. Compared with the OVAs using the high-speed PD and wideband EPMD, the proposed OVA is low-cost and has a high signal-to-noise ratio (SNR) in theory. Since the frequency of the IF photocurrent due to the beating

Manuscript received September 17, 2021; revised December 11, 2021; accepted December 13, 2021. Date of publication December 20, 2021; date of current version January 31, 2022. This work was supported by the National Key Research and Development Program of China under Grant 2018YFB2201803. *(Corresponding author: Shilong Pan.)*

The authors are with the Key Laboratory of Radar Imaging and Microwave Photonics, Ministry of Education, Nanjing University of Aeronautics and Astronautics, Nanjing 210016, China (e-mail: pans@nuaa.edu.cn).

Color versions of one or more figures in this letter are available at https://doi.org/10.1109/LPT.2021.3136708.

Digital Object Identifier 10.1109/LPT.2021.3136708

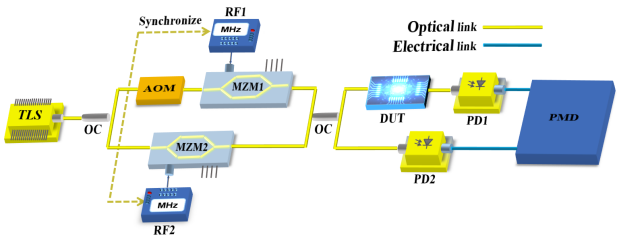

Fig. 1. Configuration of the proposed OVA. TLS: tunable laser source; OC: optical coupler; AOM: acousto-optic modulator; MZM: Mach-Zehnder modulator; DUT: device under test; RF: radio frequency; PD: photodetector; PMD: phase-magnitude detector.

of the 2nd-order sidebands is fixed and different from those beaten by other sidebands, the proposed OVA can avoid the measurement errors introduced by the 1st-order and high-order sidebands. Benefitting from utilizing the ±2nd-order sidebands, the proposed OVA can realize a wide measurement bandwidth, which is four times of the OSSB-based OVA or two times of the ODSB-based OVA. In a proof-of-concept experiment, a frequency resolution of 6 MHz and a measurement bandwidth of 120 GHz are obtained.

II. Principle

The configuration of the proposed OVA is shown in Fig. 1. To realize an OVA with wide measurement bandwidth and high resolution, the 2nd-order nonlinearity of the electro-optic modulator and microwave photonic frequency downconversion are utilized. A single frequency optical carrier ω_0 launched from a TLS is divided into two branches. In the upper branch, the optical carrier passes through an acousto-optic modulator (AOM) to introduce a frequency shift of $\Delta\omega$. Then, the frequency-shifted optical carrier is modulated by a sweeping RF signal at MZM1, which is biased at the maximum transmission point (MATP). By utilizing the 2nd-order nonlinearity of the electro-optic modulator, a pair of frequency-doubled sweeping optical signals (i.e., ±2nd-order sidebands) is generated. The optical carrier in the lower branch is modulated by another sweeping RF signal at MZM2. The RF signal has a fixed frequency interval with the RF signal driving MZM1, i.e., the two microwave signals are sweeping synchronously. Then, the two pairs of frequency-doubled sweeping optical signals are combined through an optical coupler (OC), which can be expressed mathematically as

$$\begin{aligned} E(t) = {} & A_{-2}\exp\left[i\left(\left(\omega_0+\Delta\omega\right)-2\omega_1\right)t\right]+A_{+2} \\ & \times\exp\left[i\left(\left(\omega_0+\Delta\omega\right)+2\omega_1\right)t\right] \\ & +B_{-2}\exp\left[i\left(\omega_0-2\omega_2\right)t\right]+B_{+2}\exp\left[i\left(\omega_0+2\omega_2\right)t\right] \\ & +\sum_{\substack{n=-\infty \\ n\neq -2,2}}^{n=+\infty} A_n\exp\left[i\left(\left(\omega_0+\Delta\omega\right)+n\omega_1\right)t\right] \\ & +\sum_{\substack{n=-\infty \\ n\neq -2,2}}^{n=+\infty} B_n\exp\left[i\left(\omega_0+n\omega_2\right)t\right] \end{aligned} \tag{1}$$

where ω_1 and ω_2 are the angular frequencies of the sweeping RF signals, and A_n and B_n are the complex amplitude of the nth-order sidebands of the optical signal.

One output of the OC connects to the measurement path wherein the magnitude and phase of the optical signal are changed according to the transmission function of the DUT. The propagated optical signal can be written as

$$\begin{cases} \begin{aligned} E_1(t) = {} & A_{-2}H\left[\left(\omega_0+\Delta\omega\right)-2\omega_1\right] \\ & \times\exp\left[i\left(\left(\omega_0+\Delta\omega\right)-2\omega_1\right)t\right] \\ & +B_{-2}H\left(\omega_0-2\omega_2\right)\exp\left[i\left(\omega_0-2\omega_2\right)t\right] \\ & +\sum_{\substack{n=0 \\ n\neq 2}}^{n=+\infty} A_nH\left[\left(\omega_0+\Delta\omega\right)-n\omega_1\right] \\ & \times\exp\left[i\left(\left(\omega_0+\Delta\omega\right)-n\omega_1\right)t\right] \\ & +\sum_{\substack{n=0 \\ n\neq 2}}^{n=+\infty} B_nH\left(\omega_0-n\omega_2\right)\exp\left[i\left(\omega_0-n\omega_2\right)t\right] \end{aligned} \\ \begin{aligned} E_2(t) = {} & A_{+2}H\left[\left(\omega_0+\Delta\omega\right)+2\omega_1\right] \\ & \times\exp\left[i\left(\left(\omega_0+\Delta\omega\right)+2\omega_1\right)t\right] \\ & +B_{+2}H\left(\omega_0+2\omega_2\right)\exp\left[i\left(\omega_0+2\omega_2\right)t\right] \\ & +\sum_{\substack{n=1 \\ n\neq 2}}^{n=+\infty} A_nH\left[\left(\omega_0+\Delta\omega\right)+n\omega_1\right] \\ & \times\exp\left[i\left(\left(\omega_0+\Delta\omega\right)+n\omega_1\right)t\right] \\ & +\sum_{\substack{n=1 \\ n\neq 2}}^{n=+\infty} B_nH\left(\omega_0+n\omega_2\right)\exp\left[i\left(\omega_0+n\omega_2\right)t\right] \end{aligned} \end{cases} \tag{2}$$

where $E_1(t)$ and $E_2(t)$ represent the negative and positive sidebands, $H(\omega) = H_{\mathrm{DUT}}(\omega)\cdot H_{\mathrm{sys}}(\omega)$, and $H_{\mathrm{DUT}}(\omega)$ and $H_{\mathrm{sys}}(\omega)$ are the transmission functions of the DUT and the measurement system, respectively.

After square-law detection in a low-speed PD (PD1), the probe light is converted into an IF photocurrent with a fixed frequency of $\Delta\omega+2(\omega_2-\omega_1)$ and $\Delta\omega-2(\omega_2-\omega_1)$ (assuming $\omega_2>\omega_1$, $\Delta\omega>2(\omega_2-\omega_1)$). According to (2), the frequency of the IF photocurrent is different from those generated by the 1st-order and high-order sidebands, which avoids frequency aliasing. Then a low-speed EPMD working at $\Delta\omega+2(\omega_2-\omega_1)$ or $\Delta\omega-2(\omega_2-\omega_1)$ is employed to extract the magnitude and phase information of the DUT, which can be written as

$$\begin{cases} \begin{aligned} i_{\mathrm{mea}}\left(\Delta\omega+2\left(\omega_2-\omega_1\right)\right) = {} & \eta A_{-2}B_{-2}^{*}H\left(\left(\omega_0+\Delta\omega\right)-2\omega_1\right) \\ & \times H^{*}\left(\omega_0-2\omega_2\right) \end{aligned} \\ \begin{aligned} i_{\mathrm{mea}}\left(\Delta\omega-2\left(\omega_2-\omega_1\right)\right) = {} & \eta A_{+2}B_{+2}^{*}H\left(\left(\omega_0+\Delta\omega\right)+2\omega_1\right) \\ & \times H^{*}\left(\omega_0+2\omega_2\right) \end{aligned} \end{cases} \tag{3}$$

where η is the responsivity of PD1.

In the reference path, the probe light is directly sent to another PD (PD2), wherein $H_{\mathrm{DUT}}(\omega)=1$. Thereby, the transmission function of the measurement system, i.e., $H_{\mathrm{sys}}(\omega)$, can be obtained

$$\begin{cases} \begin{aligned} i_{\mathrm{sys}}\left(\Delta\omega+2\left(\omega_2-\omega_1\right)\right) = {} & \eta A_{-2}B_{-2}^{*}H_{\mathrm{sys}}\left(\left(\omega_0+\Delta\omega\right)-2\omega_1\right) \\ & \times H_{\mathrm{sys}}^{*}\left(\omega_0-2\omega_2\right) \end{aligned} \\ \begin{aligned} i_{\mathrm{sys}}\left(\Delta\omega-2\left(\omega_2-\omega_1\right)\right) = {} & \eta A_{+2}B_{+2}^{*}H_{\mathrm{sys}}\left(\left(\omega_0+\Delta\omega\right)+2\omega_1\right) \\ & \times H_{\mathrm{sys}}^{*}\left(\omega_0+2\omega_2\right) \end{aligned} \end{cases} \tag{4}$$

Since the frequency interval between the frequency-swept dual-tone signal is much less than the bandwidth of the DUT,

the magnitude changes of the dual-tone signal can be regarded as the same and the phase changes are assumed to be linear. According to (3) and (4), the magnitude response and group delay function of the DUT can be obtained via (5) and (6), where arg(·) is a function to extract the phase of the complex amplitude in radians

$$\begin{cases} \left|H_{\mathrm{DUT}}\left(\omega_0+\dfrac{\Delta\omega}{2}-\omega_1-\omega_2\right)\right| \\ \quad \simeq \sqrt{\left|H_{\mathrm{DUT}}\left((\omega_0+\Delta\omega)-2\omega_1\right)H^{*}_{\mathrm{DUT}}\left(\omega_0-2\omega_2\right)\right|} \\ \quad = \sqrt{\left|\dfrac{i_{\mathrm{mea}}\left(\Delta\omega+2\left(\omega_2-\omega_1\right)\right)}{i_{\mathrm{sys}}\left(\Delta\omega+2\left(\omega_2-\omega_1\right)\right)}\right|} \\ \left|H_{\mathrm{DUT}}\left(\omega_0+\dfrac{\Delta\omega}{2}+\omega_1+\omega_2\right)\right| \\ \quad \simeq \sqrt{\left|H_{\mathrm{DUT}}\left((\omega_0+\Delta\omega)+2\omega_1\right)H^{*}_{\mathrm{DUT}}\left(\omega_0+2\omega_2\right)\right|} \\ \quad = \sqrt{\left|\dfrac{i_{\mathrm{mea}}\left(\Delta\omega-2\left(\omega_2-\omega_1\right)\right)}{i_{\mathrm{sys}}\left(\Delta\omega-2\left(\omega_2-\omega_1\right)\right)}\right|} \end{cases} \tag{5}$$

$$\begin{cases} \tau\left(\omega_0+\dfrac{\Delta\omega}{2}-\omega_1-\omega_2\right) \\ =\dfrac{\arg\left[H_{\mathrm{DUT}}((\omega_0+\Delta\omega)-2\omega_1)\right]-\arg\left[H_{\mathrm{DUT}}\left(\omega_0-2\omega_2\right)\right]}{\Delta\omega+2\left(\omega_2-\omega_1\right)} \\ =\arg\left[\dfrac{i_{\mathrm{mea}}\left(\Delta\omega+2\left(\omega_2-\omega_1\right)\right)}{i_{\mathrm{sys}}\left(\Delta\omega+2\left(\omega_2-\omega_1\right)\right)}\right]\Big/\left(\Delta\omega+2\left(\omega_2-\omega_1\right)\right) \\ \tau\left(\omega_0+\dfrac{\Delta\omega}{2}+\omega_1+\omega_2\right) \\ =\dfrac{\arg\left[H_{\mathrm{DUT}}((\omega_0+\Delta\omega)+2\omega_1)\right]-\arg\left[H_{\mathrm{DUT}}\left(\omega_0+2\omega_2\right)\right]}{\Delta\omega-2\left(\omega_2-\omega_1\right)} \\ =\arg\left[\dfrac{i_{\mathrm{mea}}\left(\Delta\omega-2\left(\omega_2-\omega_1\right)\right)}{i_{\mathrm{sys}}\left(\Delta\omega-2\left(\omega_2-\omega_1\right)\right)}\right]\Big/\left(\Delta\omega-2\left(\omega_2-\omega_1\right)\right). \end{cases} \tag{6}$$

III. Experiment Results and Discussion

An experiment based on the configuration in Fig. 1 is carried out. An optical carrier with a wavelength of 1547.148 nm is generated by a tunable laser source (TLS, TeraXion PS-TNL) and divided into two branches. The optical carrier in the upper branch is shifted by an acousto-optic modulator (AOM, Gooch & Housego T-M200-0.1C2J-3-F2P) with a fixed frequency of 150 MHz. Then, the frequency-shifted optical carrier is modulated by a sweeping RF signal (RF1) at MZM1 (Fujitsu FTM7938EZ) working at the MATP to generate a pair of frequency-doubled sweeping optical signals. The other part of the optical carrier undergoes a similar modulation at MZM2 (Fujitsu FTM7938EZ) driven by another sweeping RF signal (RF2), which has a fixed frequency interval of 10 MHz with RF1. Then the generated two pairs of frequency-doubled sweeping optical signals are combined and measured by a high-resolution optical spectrum analyzer (OSA, APEX AP2040D). Due to the power of the probe light is small, which results in a poor SNR of the frequency response. To improve the power of the probe light, a programmable optical filter (POF, Finisar WaveShaper 4000s) is used to extract a pair of frequency-swept dual-tone signals (i.e., two -2nd-order sidebands). The filtered signal is amplified by the following EDFA and then sent to the optical band-pass filter (OBPF, Pritel TFA-1550) to remove the out-of-band noise. A $H^{13}C^{14}N$ gas cell (Wavelength References HCN-13-H(16.5)-25-FCAPC) serves as the DUT. Two photodetectors (PD, THORLABS PDB450C-AC) are inserted to convert the probe light into an IF photocurrent with a fixed frequency. An electrical vector network analyzer (EVNA, Keysight N5235A) working at the same frequency as the IF photocurrent serves as the electrical phase-magnitude detector (EPMD) to extract the magnitude and phase of the IF photocurrent in the measurement path according to the reference path. Then, the center wavelength of the POF is changed to filter out another pair of frequency-swept dual-tone signals (i.e., two +2nd-order sidebands) and the same operation as above is performed.

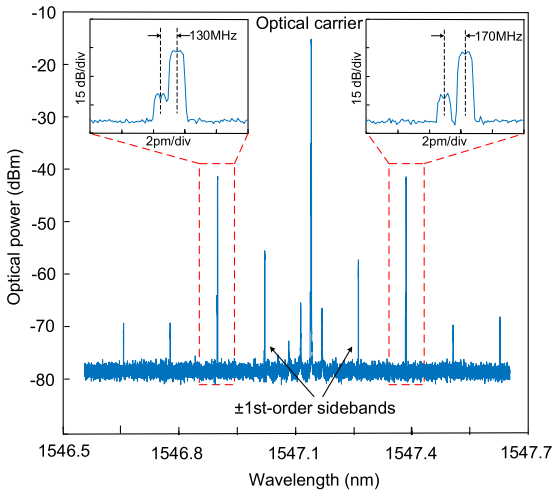

Fig. 2. Optical spectrum of the combined optical signal.

Figure 2 shows the optical spectrum of the combined optical signal when two RF signals with frequencies of 15 and 15.01 GHz are injected into the two MZMs. As can be seen, two pairs of frequency-swept dual-tone signals having fixed frequency intervals of 130 and 170 MHz are generated, as shown in the insets of Fig. 2. The fixed frequency intervals between the probe light are different from those between the 1st-order and high-order sidebands. A low-speed EMPD working at 170 and 130 MHz is employed, the frequency components generated by the undesired sidebands can be filtered out and thus have no influence on the measurement results.

Figure 3 shows the measured magnitude and group delay responses of the $H^{13}C^{14}N$ gas cell, which is achieved by sweeping the microwave signal from 5 to 35 GHz with a sweeping interval of 3 MHz. Therefore, the measurement bandwidth is 120 GHz (−70∼−10 GHz and 10∼70 GHz offset the optical carrier) with a frequency resolution of 6 MHz. The discontinuity of the responses in the frequency range of 20 GHz (−10∼10 GHz offset the optical carrier) is caused by the edge effect of the POF. If a band-stop filter with ultranarrow bandwidth and steep edges is used to remove the optical carriers, the discontinuity can be removed. As a comparison, the magnitude response of the DUT measured by the OSA with a resolution of 6 MHz is also plotted in Fig.3. As can be seen, the two amplitude response curves are in good agreement, and the proposed OVA has a higher signal-to-noise ratio (SNR).

To investigate the influence of the frequency interval between the frequency-swept dual-tone signal on the group delay response measurement accuracy, a numerical simulation

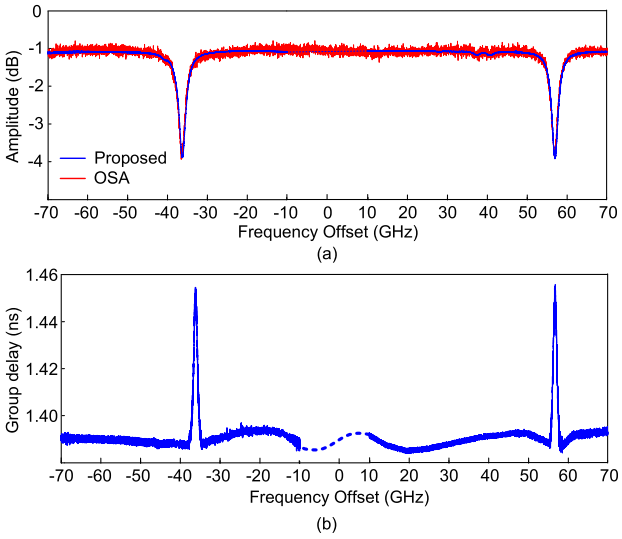

Fig. 3. (a) Magnitude and (b) group delay responses of the $H^{13}C^{14}N$ gas cell.

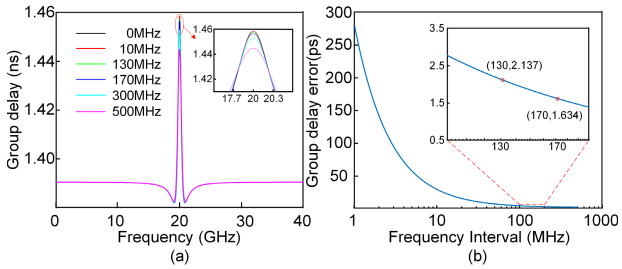

Fig. 4. Numerical simulation of (a) the group delay responses and (b) the group delay error under different frequency intervals.

is performed. The measurement accuracy comprises trueness and precision. For the measurement trueness, when the frequency interval grows, the assumption of (6) that the phase changes of the dual-tone signal are linear is no longer valid. As can be seen in Fig. 4(a), the deviation between the measured value and the theoretical value at the absorption peak of the $H^{13}C^{14}N$ gas cell increases with the growth of the frequency interval. Therefore, the frequency interval should be as small as possible to realize high measurement trueness. On the other hand, the measurement precision is severely affected by the phase measurement errors of the EMPD with the decrease of the frequency interval. According to (6), the group delay response error is given by $\Delta\tau = \Delta\phi/\Omega$, where $\Delta\phi$ is the phase measurement error of the EMPD (set to 0.1°), and Ω is the frequency interval of the dual-tone signal. As shown in Fig. 4(b), the group delay error is inversely proportional to the frequency interval. Hence, in order to ensure the precision of the group delay response, the frequency interval should not be too small. Therefore, frequency intervals of 130 and 170 MHz are selected, in which the deviation of measurement trueness is less than 2.28 ps at the absorption peak and the error of measurement precision is less than 2.137 ps.

IV. Conclusion

In conclusion, a novel method to perform a high-resolution and wideband OVA based on microwave photonic frequency downconversion is proposed and experimentally demonstrated. Compared with the OVAs using high-speed PDs and wideband EPMDs, the proposed OVA is low-cost and has a high SNR. Utilizing the 2nd-order nonlinearity of the electro-optic modulation, the proposed OVA achieves wide measurement bandwidth, which is four times of the OSSB-based OVA or two times of the ODSB-based OVA. The magnitude and group delay responses of the $H^{13}C^{14}N$ gas cell are obtained within the frequency range of 120 GHz, and the frequency resolution is 6 MHz. The influence of the frequency interval between the frequency-swept dual-tone signal on the measurement accuracy of the group delay response is investigated through numerical simulation.

References

[1] G. D. VanWiggeren, A. R. Motamedi, and D. M. Barley, "Single-scan interferometric component analyzer," *IEEE Photon. Technol. Lett.*, vol. 15, no. 2, pp. 263–265, Feb. 2003.

[2] M. Volanthen, H. Geiger, M. J. Cole, R. I. Laming, and J. P. Dakin, "Low coherence technique to characterise reflectivity and time delay as a function of wavelength within a long fibre grating," *Electron. Lett.*, vol. 32, no. 8, pp. 757–758, Apr. 1996.

[3] S. Ryu, Y. Horiuchi, and K. Mochizuki, "Novel chromatic dispersion measurement method over continuous Gigahertz tuning range," *J. Lightw. Technol.*, vol. 7, no. 8, pp. 1177–1180, Aug. 15, 1989.

[4] G. Genty, T. Niemi, and H. Ludvigsen, "New method to improve the accuracy of group delay measurements using the phase-shift technique," *Opt. Commun.*, vol. 204, nos. 1–6, pp. 119–126, Apr. 2002.

[5] W. Chen, M. Xue, D. Zhu, C. Yu, and S. Pan, "Optical vector analysis with improved accuracy and enhanced dynamic range," *IEEE Photon. Technol. Lett.*, vol. 31, no. 19, pp. 1565–1568, Oct. 1, 2019.

[6] M. Sagues and A. Loayssa, "Swept optical single sideband modulation for spectral measurement applications using stimulated Brillouin scattering," *Opt. Exp.*, vol. 18, no. 16, pp. 17555–17568, Aug. 2010.

[7] Z. Tang, S. Pan, and J. Yao, "A high resolution optical vector network analyzer based on a wideband and wavelength-tunable optical single-sideband modulator," *Opt. Exp.*, vol. 20, no. 6, pp. 6555–6560, Mar. 2012.

[8] L. Li, X. Yi, S. X. Chew, S. Song, L. Nguyen, and R. Minasian, "High-resolution optical vector network analyzer based on silicon-on-insulator coupled-resonator optical waveguides," in *Proc. 22nd Int. Conf. Appl. Electromagn. Commun. (ICECOM)*, Sep. 2016, pp. 1–4.

[9] S. Pan and M. Xue, "Ultrahigh-resolution optical vector analysis based on optical single-sideband modulation," *J. Lightw. Technol.*, vol. 35, no. 4, pp. 836–845, Feb. 15, 2017.

[10] S. X. Chew *et al.*, "Silicon-on-insulator dual-ring notch filter for optical sideband suppression and spectral characterization," *J. Lightw. Technol.*, vol. 34, no. 20, pp. 4705–4714, Oct. 15, 2016.

[11] M. Wang and J. Yao, "Optical vector network analyzer based on unbalanced double-sideband modulation," *IEEE Photon. Technol. Lett.*, vol. 25, no. 8, pp. 753–756, Apr. 15, 2013.

[12] W. Jun *et al.*, "Optical vector network analyzer based on double-sideband modulation," *Opt. Lett.*, vol. 42, no. 21, pp. 4426–4429, Nov. 2017.

[13] X. Zou *et al.*, "Hyperfine intrinsic magnitude and phase response measurement of optical filters based on electro-optical harmonics heterodyne and Wiener–Lee transformation," *J. Lightw. Technol.*, vol. 37, no. 11, pp. 2654–2660, Jun. 1, 2019.

[14] T. Qing, S. Li, Z. Tang, B. Gao, and S. Pan, "Optical vector analysis with attometer resolution, 90-dB dynamic range and THz bandwidth," *Nature Commun.*, vol. 10, no. 1, p. 5135, Dec. 2019.